Study on structure and photoluminescence properties of hydrated phase halides solid solution

$$Rb_2InCl_xBr_{(5-x)} \cdot H_2O{:}Sb$$

Undergraduate Research Thesis

Presented in partial fulfillment of the requirements for graduation

with honors research distinction in Chemistry in the College of Art and Science of The Ohio State University

by

Ye Wang

The Ohio State University

May 2022

Project Advisor: Professor Patrick Woodward, Department of Chemistry and Biochemistry

1. **Abstract**
2. **Introduction**
    a. General introduction
    b. Hydrated phase materials
    c. Halide solid solution
    d. Research purpose
3. **Experimental:**
    a. Synthesis
    b. X-ray Diffraction
    c. Fluorescence Spectroscopy
4. **Results**
    a. XRD pattern
    b. Crystal structure
    c. Crystal parameters
    d. Photoluminescence properties
5. **Discussion**
    a. Analysis XRD patterns and refinements
    b. Crystal structure information
    c. Photoluminescence Properties
6. **Conclusion**
7. **Reference**

1. Abstract:

In this research, the crystal structural information and photoluminescence properties related to changing the ratio of halide X (Cl and Br) in the $Rb_2InX_5 \cdot H_2O$: Sb^{3+} materials were studied. Samples of $Rb_2InCl_xBr_{(5-x)} \cdot H_2O$: Sb 5% were prepared at x values ranging from 0 to 5 from hydrothermal reaction conditions in hydrohalic acid. Based on Rietveld refinements, the general crystal structure change did not follow a Vegard's Law transition and the smaller Cl anion was favored in the structure, especially favored at the Wyckoff site 8d in the unit cell. The effect of coordinated water molecules on the preferential substitution of the halides was explored. PL emission maximum also trends with halide substitution with a red shift as Br is introduced. The highest intensity of emission was found for $Rb_2InCl_1Br_5 \cdot H_2O$: Sb^{3+} with an emission maximum around 700 nm with a PLE maximum at 360 nm.

2. Introduction:

a. General introduction:

As a material with great potential in photoluminescence and magnetic properties, perovskites, with the basic formula of ABX_3 (A = +1 cation, B = +2 cation, and X = -1 anion), and perovskites derivatives were widely studied in the past. Different structure types of perovskites were synthesized and analyzed, including double perovskites, triple perovskites, and vacancy perovskites. One of the promising perovskites was lead perovskites, which shared many interesting properties. However, although halide perovskites with lead showed great efficiency and potential in photoluminescence properties, they were toxic and environmentally unfriendly due to the presence of lead. As a result, finding the replacement of lead in perovskites structure

and studying the photoluminescence properties of these lead-free perovskites were important topics in this field.

b. Hydrated phase materials:

Hydrated phase materials, which share a formula of $A_2BX_5 \cdot H_2O: Sb$, are a type of zero-dimensional perovskites. Zero-dimensional perovskites are perovskites derivatives, which share a formula of A_4BX_6, such as Cs_2SnX_6. In the crystal structure of 0D perovskites, the octahedra clusters $[BX_6]^{4-}$ are isolated from each other by the surrounding cations. This structural feature provides some unique electron and photoluminescence characters.

In the crystal structures of hydrated phase materials, one of anions of the A_2BX_6 system was replaced by H_2O molecule while the oxidation state of the B-site cation is reduced from 4+ to 3+ such as the case $[Sn^{4+}\ X_6]^{2-}$ going to $[In^{3+}X_5H_2O]$. The hydrated phase materials may provide a platform for high efficiency luminescent systems while avoiding the presence of toxic Pb. For example, $Rb_2InCl_5 \cdot H_2O: Sb\ 1\%$ and $Cs_2InCl_5 \cdot H_2O: Sb\ 1.5\%$ shared high external photoluminescence quantum efficiency (50.8% for $Rb_2InCl_5 \cdot H_2O: Sb\ 1\%$ and 72.8% for $Cs_2InCl_5 \cdot H_2O: Sb\ 1.5\%$). This indicates that hydrated phase materials could be potential materials with high efficiency which may be potential alternatives to Lead perovskites systems.

c. Halides solid solution:

Solid solution involving with mixing sites and alloying in sites is a method to tune the crystal structures and properties of the material by combining either same charged cations (anions) or differently charged cations with average expected charges at certain site. This provides great flexibility for the application of materials. For example, photoluminescence properties of perovskites can be tuned to certain excitation and emission between two end

members. Atoms serve as electron acceptors and donors can also be added to the crystal structure to enable electrons transfer for photoluminescence. There has been much study on certain types and synthesis of perovskites with mixing sites (halides) and alloying sites for photoelectric and photoluminescence properties. However, there are not many studies on the crystal structural change during mixing and alloying for perovskites, which may be useful for understanding the structural properties in the mixing and alloying process from one end member to another.

d. Research purpose:

In this research, the hydrated phase materials studied are $Rb_2InCl_xBr_{(5-x)} \cdot H_2O$: Sb 5%. There are two major parts in this research. One is how the crystal structure changes as the halide composition altered across the solid solution. The presence of a coordinated water molecule in the octahedral unit may cause preferential halide substitution due to the difference in bonding abilities related to cis- and trans- electronic effects. The other is studying the photoluminescence properties at the different halide ratios. As the photoluminescence properties of both end members have been published, the research should focus on the trend between the two endmembers. A potential halides ratio should be figured out for potential high efficiency replacement at the excitation wavelength (around 365 nm) of current commercial applications.

3. Experimental:

a. Synthesis:

The synthesis of $Rb_2InCl_xBr_{(5-x)} \cdot H_2O: Sb$ 5% samples were based on hydrothermal reactions. The reaction was based on equation 1. To produce products (targeted mass = 1.7g) with different halide ratios, the moles of Cl and Br ions from hydrochloride and hydrobromide acid were calculated to match the ratio of the halide ratio in the products.

Equation 1:

$$4RbCl + In_2O_3(Sb_2O_3) + 6HCl/HBr \xrightarrow{110℃/53h} 2Rb_2InCl_xBr_{(5-x)} \cdot H_2O: Sb + H_2O$$

$RbCl$, In_2O_3 and Sb_2O_3 with calculated mass were weighed and added into Teflon Liner. After adding HCl and HBr (total 8 mL, Table 1), H_2O (2 mL) and H_3PO_2 (0.5 mL), the Teflon Liners were set to stir for 10 minutes to dissolve the reagents. The Teflon Liners were then packed and placed in the oven. The reaction condition was set to be at 110 °C for 24 hours, with a ramp rate of 100 °C per hour on heating and a ramp rate of -3 °C per hour on cooling. The crystalline products were washed with ethanol and dried under vacuum. The products were grounded and stored.

Table 1. Hydrohalic acid volume in synthesis

	The expected molar ratio (Cl:Br):	Volume of HCl (12M) (mL):	Volume of HBr (8.84M) (mL):
$Rb_2InClBr_4 \cdot H_2O$: Sb	1:4	1.23	6.77
$Rb_2InCl_2Br_3 \cdot H_2O$: Sb	2:3	2.62	5.38
$Rb_2InCl_3Br_2 \cdot H_2O$: Sb	3:2	4.18	3.82
$Rb_2InCl_4Br \cdot H_2O$: Sb	4:1	5.96	2.04

b. X-ray Diffraction:

The XRD data of the powder samples was collected from the Bruker XRD and refined with TOPAS. The XRD scanning was set with the scanning rate of 1 degree per minute from 10 degrees to 60 degrees 2θ. The Rietveld refinement of the data was performed to determine the unit cell information and crystallographic positions of the atoms in the unit cell.

c. Fluorescence Spectroscopy:

The Powder samples photoluminescence properties were collected using Fluorescence Spectroscopy. The background information was collected before each measurement with a lab reflectance standard for both excitation and emission measurements. The emission spectra were collected with an excitation wavelength of 365 nm from 450 nm to 800 nm. The excitation was collected at the highest peak of sample emissions from 250 nm to 380 nm with the detecting wavelength at maximum emission for each sample. The background was reduced for accuracy of the data. Both excitation and emission patterns were normalized to determine the photoluminescence changes based on different halide ratios.

4. Results:

a. XRD pattern:

Figure 1. X-Ray Diffraction patterns of samples $Rb_2InCl_xBr_{(5-x)} \cdot H_2O$: Sb

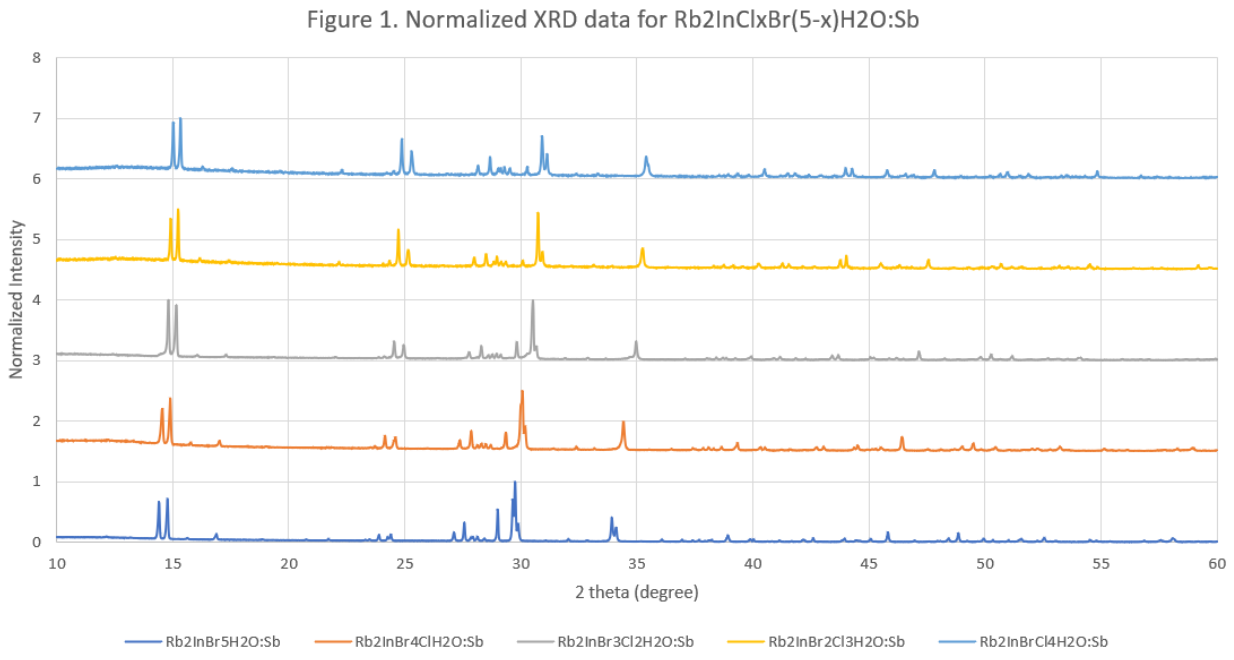

Figure 2. X-Ray Diffraction patterns of samples $Rb_2InCl_xBr_{(5-x)} \cdot H_2O$: Sb (Zoomed at 10°-16°)

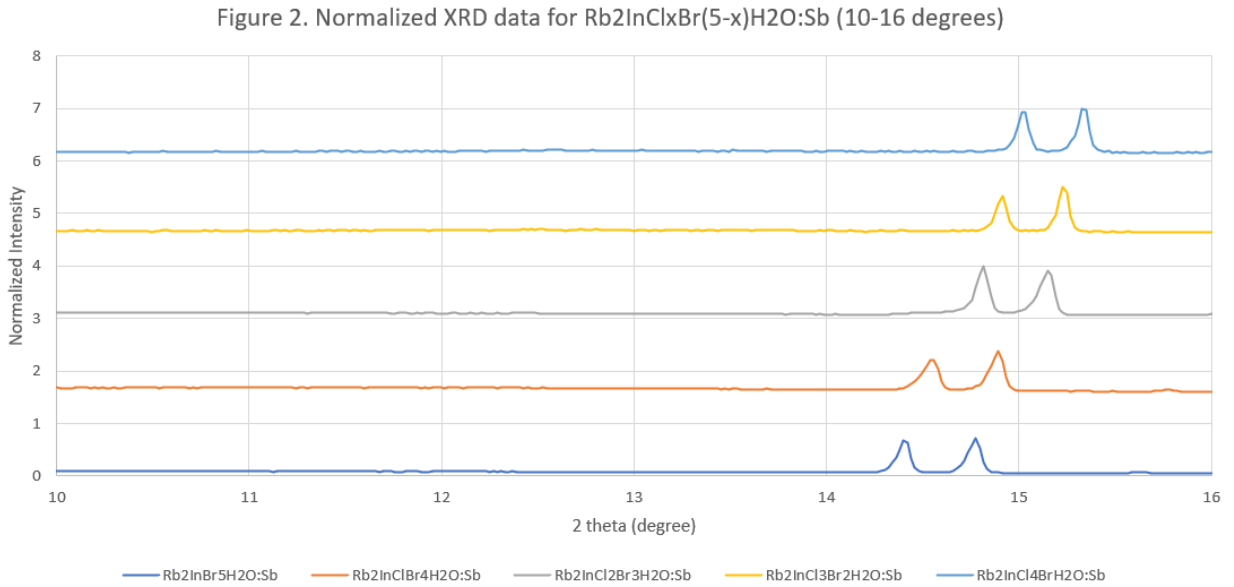

b. Crystal structure:

Figure 3. Refined crystal structure of sample $Rb_2InCl_2Br_3 \cdot H_2O$: Sb (H atoms were removed for clarity.)

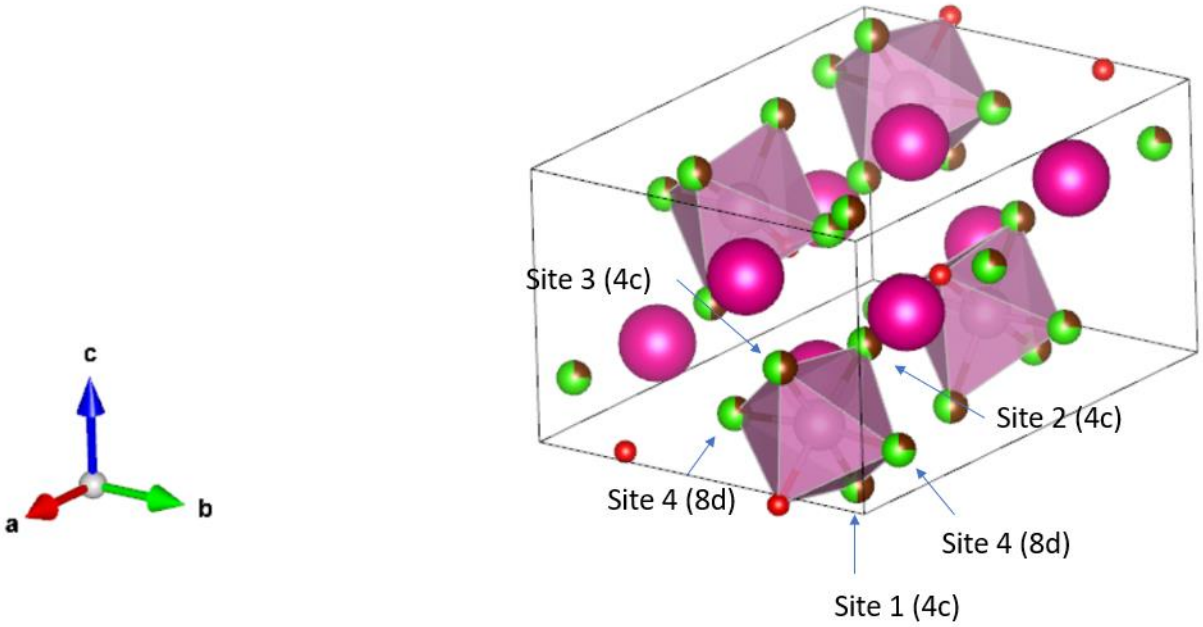

c. Crystal parameter:

The crystal parameters and halides ratios were refined from the XRD patterns. The refined Br coefficient was calculated based on the total number of Br atoms refined in a unit cell and divided by Z value (Z = 4).

Table 2. Crystal parameter information of samples $Rb_2InCl_xBr_{(5-x)} \cdot H_2O{:}\,Sb$

Sample:	x (Å):	y (Å):	z (Å):	Unit cell volume ($Å^3$):	Expected Br coefficient (5-x):	Refined Br coefficient:
$Rb_2InClBr_4 \cdot H_2O{:}\,Sb$	14.45298 ± 0.000267	10.41162 ± 0.000200	7.487359 ± 0.000124	1126.68(9)	4	3.9
$Rb_2InCl_2Br_3 \cdot H_2O{:}\,Sb$	14.29154 ± 0.000413	10.27551 ± 0.000259	7.38772 ± 0.000233	1084.90(1)	3	1.9
$Rb_2InCl_3Br_2 \cdot H_2O{:}\,Sb$	14.16565 ± 0.000364	10.18958 ± 0.000235	7.310515 ± 0.000206	1055.21(2)	2	1.0
$Rb_2InCl_4Br \cdot H_2O{:}\,Sb$	14.10044 ± 0.000283	10.15001 ± 0.000195	7.26875 ± 0.000159	1040.30(1)	1	0.8

Table 3. Refined ratio and components in crystal structures of samples $Rb_2InCl_xBr_{(5-x)} \cdot H_2O$: Sb

Sample:	Br on Site 1 (4):	Br on Site 2 (4):	Br on Site 3 (4):	Br on Site 4 (8d):
$Rb_2InClBr_4 \cdot H_2O$: Sb	1 ± 0.04135	1 ± 0.04079	0.9478 ± 0.02387	0.5 ± 0.02075
$Rb_2InCl_2Br_3 \cdot H_2O$: Sb	0.5048 ± 0.0401	0.41755 ± 0.03741	0.48339 ± 0.04871	0.26101 ± 0.02235
$Rb_2InCl_3Br_2 \cdot H_2O$: Sb	0.20288 ± 0.02571	0.25909 ± 0.02789	0.28804 ± 0.03074	0.14949 ± 0.01662
$Rb_2InCl_4Br \cdot H_2O$: Sb	0.14897 ± 0.02668	0.26462 ± 0.02972	0.15941 ± 0.02972	0.11611 ± 0.01683

Figure 4. Unit cell volumes of samples $Rb_2InCl_xBr_{(5-x)} \cdot H_2O$: Sb

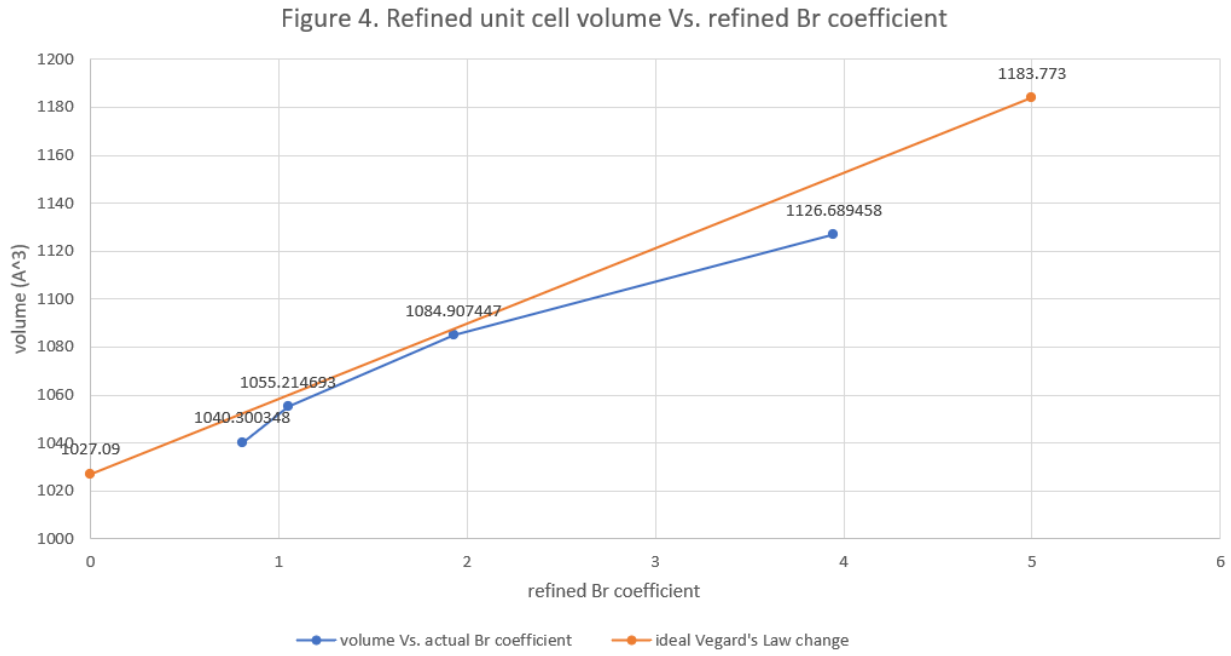

Figure 5. Br component percentage on each Wyckoff site

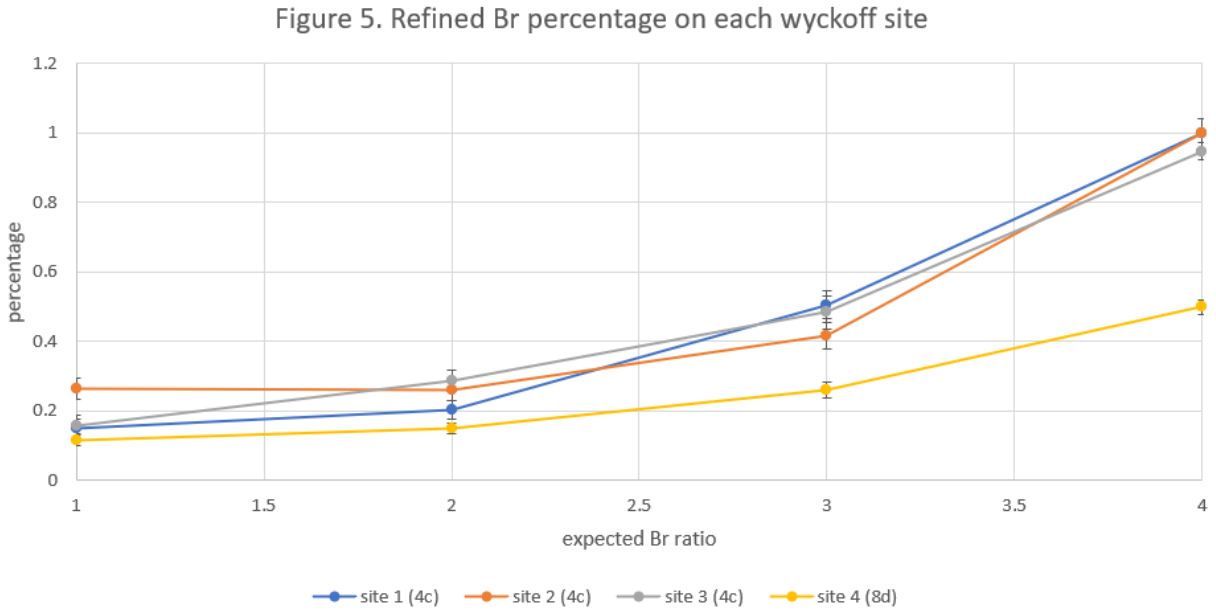

Figure 6. Cl component percentage on each Wyckoff site

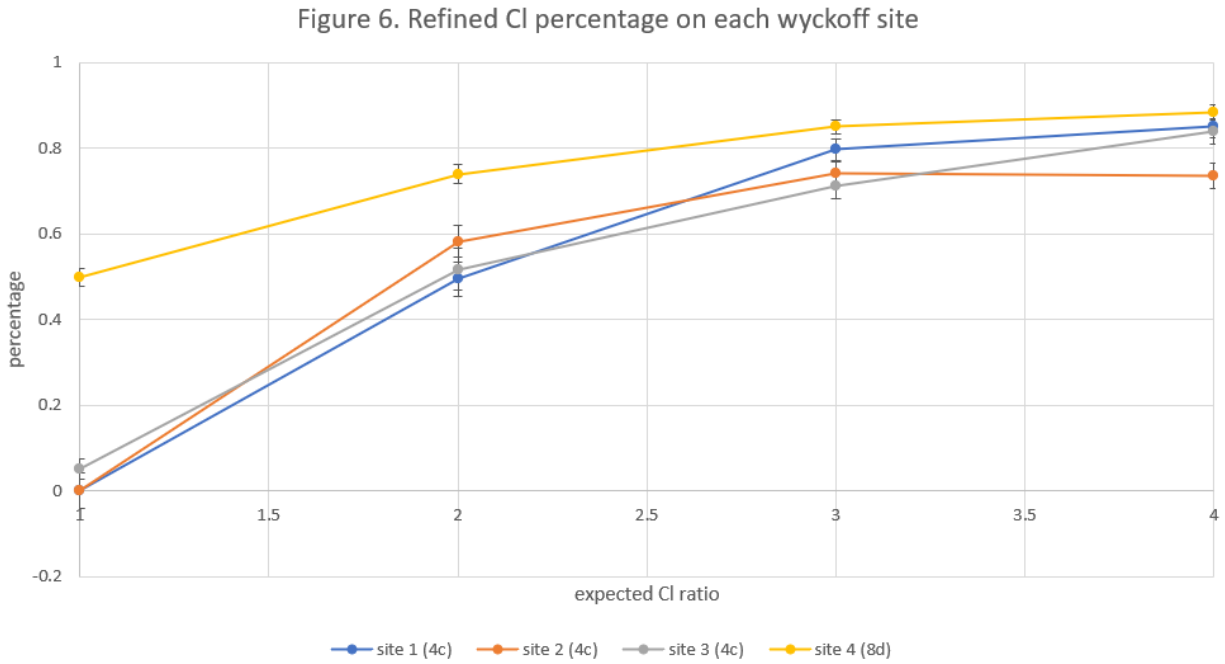

d. Photoluminescence Properties:

Photoluminescence Excitation:

Figure 7. Normalized photoluminescence excitation of samples $Rb_2InCl_xBr_{(5-x)} \cdot H_2O: Sb$

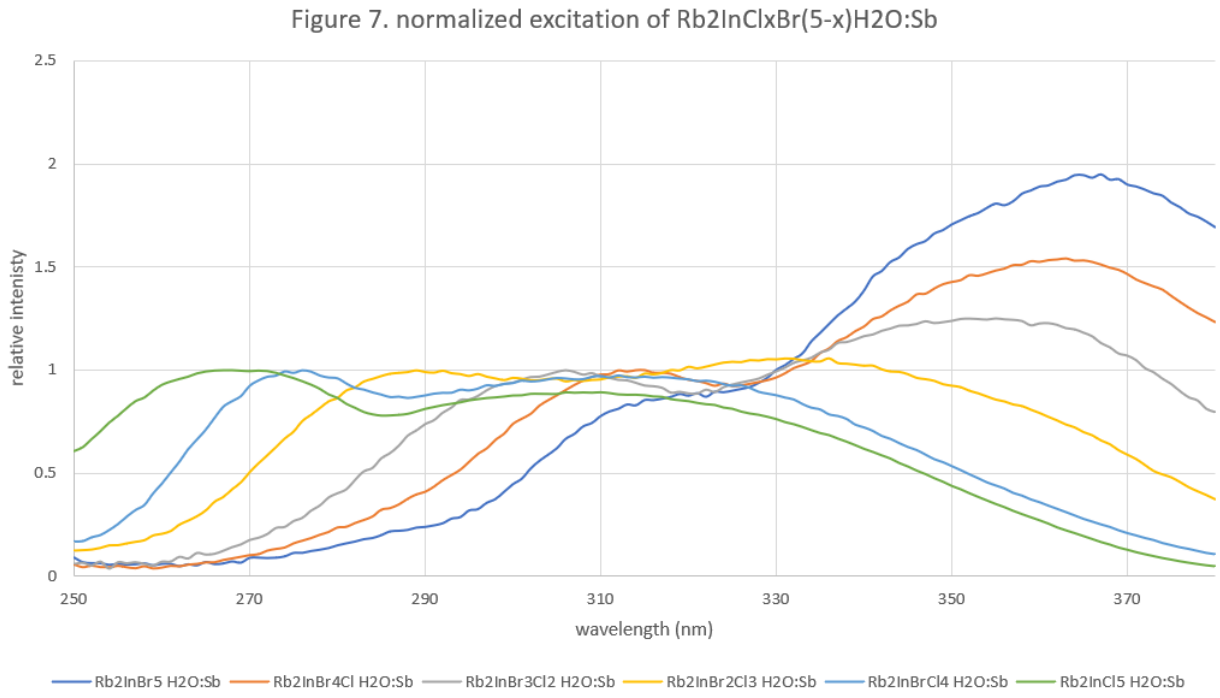

Photoluminescence Emission:

Figure 8. Photoluminescence emission of samples $Rb_2InCl_xBr_{(5-x)} \cdot H_2O$: Sb

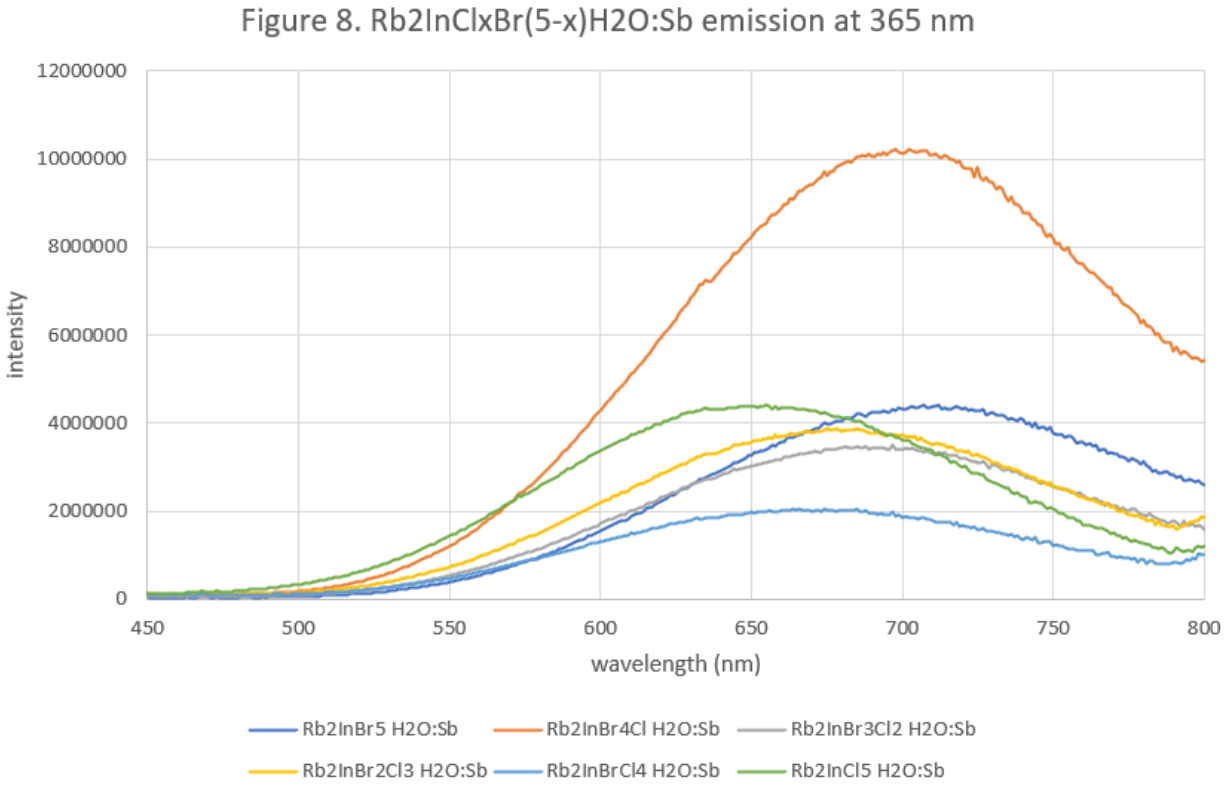

Figure 9. Normalized photoluminescence emission of samples $Rb_2InCl_xBr_{(5-x)} \cdot H_2O$: Sb

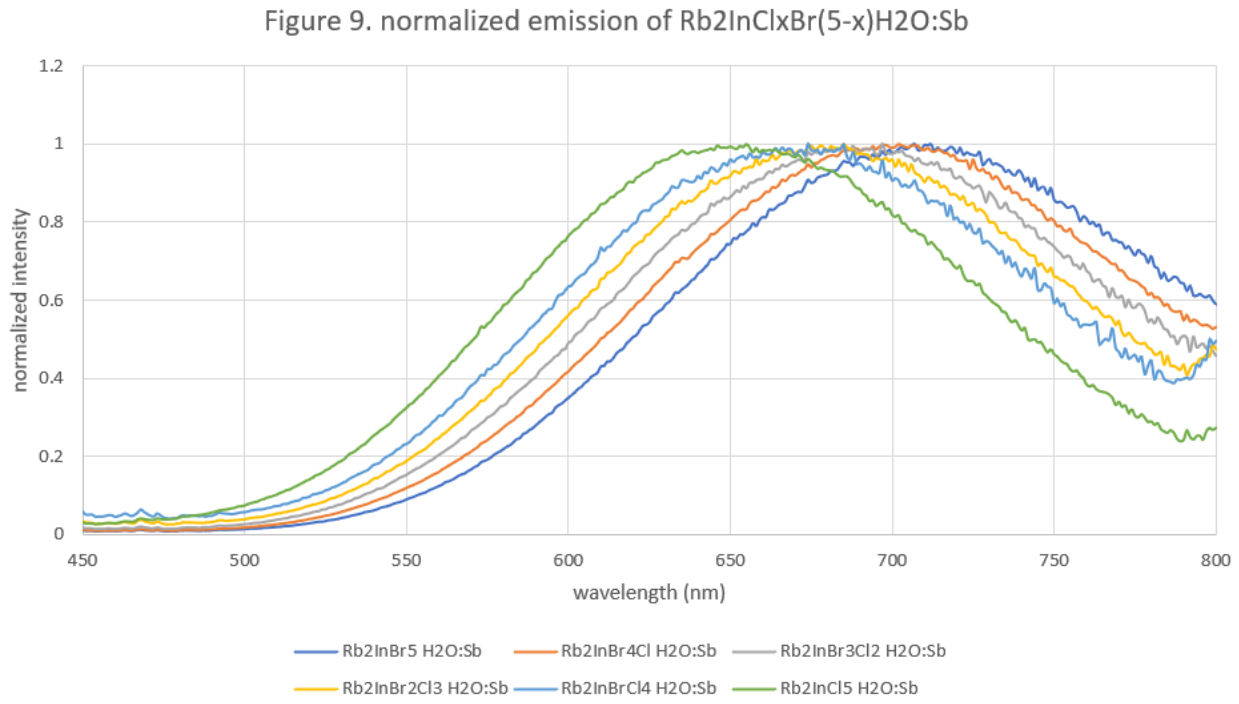

Figure 10. the emission maximum wavelength of each sample at certain refined Br coefficients

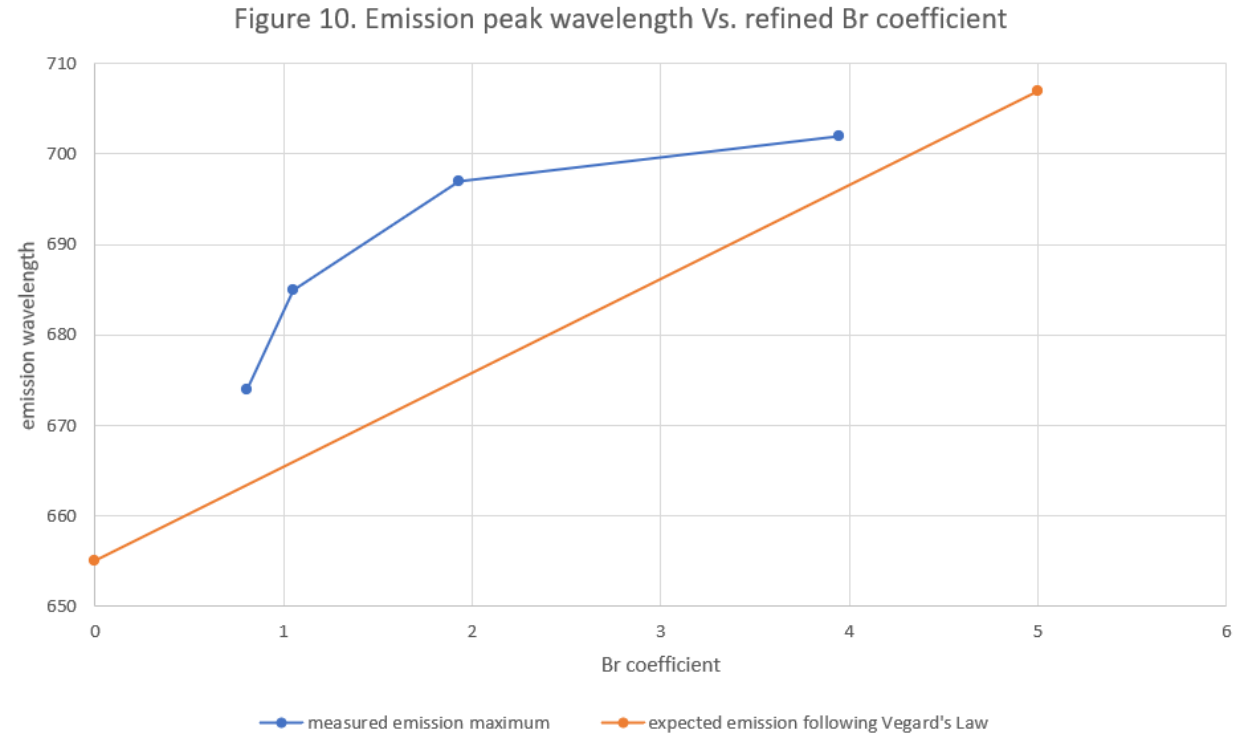

5. Discussion:

a. XRD patterns and refinements:

The XRD patterns were collected for a set of samples with expected round numbers of halides ratios from $Rb_2InCl_4Br \cdot H_2O{:}\,Sb$ to $Rb_2InBr_5 \cdot H_2O{:}\,Sb$. The Normalized XRD patterns were showed in Figure 1. Based on Figure 1, the crystal structure information could be figured out that the XRD patterns shifted to lower angles with increasing in the bromine content. This indicated a basic idea that the samples with higher Br content in halides ratio had larger unit cell volume, as Br possessed a larger radius than Cl did.

In the refinements of XRD data, all the XRD patterns fitted in the pattern of space group Pnma without additional peak, which indicated that there was no impurity and mixing phase in the sample crystals when the halides ratios were changed. During the refinements, the Wyckoff sites for each component were collected, especially for Br and Cl, to study how different coordinated halides change in the unit cell by comparing each sample. The halides occupied three different positions with site 4c symmetry, which shared a y coordinate of $\frac{1}{4}$, and one position with site 8d symmetry, which shared randomized x, y, and z coordinates. The total number of halides was 20 in each unit cell. The occupancies of Br and Cl at different sites were collected in Table 3, which provided direct information on the average Br and Cl ratio in the unit cell.

Based on the total number of halides atoms and the occupancies of Cl and Br at each site, the refined ratios and Br and Cl coefficients were calculated and collected in Table 2. From the refined coefficient of Br in Table 2, the idea could be concluded that Cl was favored and tended to enter the structure during the crystal formation, as refined Br coefficients were always lower

than the expected coefficients. In the synthesis process, two sets of samples were synthesized with different reagents of RbCl and RbBr, as the halide ions for Rb-salts were not put into mole consideration at first. This was due to the initial focus was based on changing pattern of halides. The initial expectation for the halides was that the environmental rich halide in the synthesis solution tended to enter the structure. However, in both cases under different Cl and Br rich environments, refined Br coefficients tended to be smaller than the expectation values.

b. Crystal structure information:

The unit cell parameters from refinements were collected in Table 2. The values in all three dimensions followed the idea from the XRD patterns that the unit cell became larger with the increase of Br content. Based on the actual coefficients of halides and the unit cell parameters and the unit cell volumes in Figure 4, a conclusion could be drawn that Vegard's law was not followed. The changing pattern between coefficients and parameters was not linear. As there was no change in the oxidation states, inhomogeneities might be a possible reason why Vegard's law deviated, which led to the further study on the bandgap changing pattern. However, the reduced difference between expected volumes and refined volumes showed in Figure 4, which is the close positions of refined data points to the lines of expectation volumes, indicated that the refined halides coefficients were reliable compared to the expected coefficient.

In Figure 5 and Figure 6, the ratio of Br and Cl at each site was drawn to show whether there was a favor for a certain site to be occupied by Br or Cl. Site 8d tended to acquire more Cl than Br during the changing of halides ratios. In Figure 3, the crystal structure provided a clear image of the position of site 8d and the different occupancies at site 8d. One of the characteristics of site 8d was that it was bisected by a mirror plane. And all the other halides occupied site 4c, which lay on the mirror plane.

Although, in hydrated phase materials, water molecule replaced one of the halide atoms in the structure, it did not affect the replacements of halides at different sites based on the refined halides ratios at each site. Even if there were three sites 4c in the structure, two of which were cis site to the water molecule and one of which was trans site, the ratios at these three sites were similar to each other at the same structure.

This led to a further study about figuring out whether other hydrated phase materials followed a similar pattern in different mixing sites.

c. Photoluminescence Properties:

The photoluminescence data was collected in Figure 7 to Figure 9. For the excitation in Figure 7, there were two major peaks in the excitation pattern. With the increase Br in halides ratio, the excitation peaks shifted toward a higher wavelength and lower energy. The intensity of major peaks was also changed by different ratios. With the increase in Br, the intensity of the second peak increased and surpass the intensity of the first peak. As the second peaks of this set of samples shifted to around 350 nm with a high Br ratio, it could be a potential source for photoluminescence at the current commercial standard excitation wavelength (365 nm).

For the emission, the potential highest efficiency among all samples could be figured out in Figure 9. $Rb_2InClBr_4 \cdot H_2O{:}\,Sb$ exhibited a higher intensity emission with the same Sb-doping percentage than the other samples. The relatively high intensity of $Rb_2InClBr_4 \cdot H_2O{:}\,Sb$ compared to other samples might lead to a possible high efficiency under similar photoluminescence mechanism. However, this needed to be further confirmed by the photoluminescence quantum yield measurement in future study. From Figure 9, the peak shifting could also be concluded in emission that the increase in Br content led to the higher emission

wavelength, as expectation. In Figure 10, the peak wavelengths of emissions were drawn related to the refined Br coefficients to determine whether the photoluminescence properties followed Vegard's Law. As the changing pattern of emission was not linear or relatively linear, the photoluminescence properties did not follow Vegard's Law, which also matched the conclusions from the refined crystal parameters data that Vegard's Law was not followed for this set of materials. However, the energy of the photoluminescence needed to be further study and measurements to confirm whether the Vegard's Law was followed.

The changing pattern in Figure 10 could lead to a possible idea, related to the coordinate's information of Sb, that Br might tend to bond to Sb compared to In to form clusters in crystal structures. The reason was that the dramatic increase in wavelength at the low Br coefficients sample indicated that Br entered the structure and started to bond with Sb. As the amount of Sb was relatively small compared to In, when the coordinates of Br were mostly occupied by Br, Br started to bond with In and did not affect the emission wavelength anymore. This changing pattern matched with the pattern of wavelength change in Figure 10, in that the wavelength dramatically increased at low Br coefficients and then slowly increased at high Br coefficients. This idea also needed to be confirmed in future studies.

6. Conclusion:

A conclusion could be drawn about how the halides ratio change affected the crystal structure. In the changing of halides ratios, the crystal followed a same space group of Pnma with deviations from Vegard's Law in crystal structure and photoluminescence properties. From this we can conclude that a complete solid solution forms between $Rb_2InCl_5 \cdot H_2O$ and $Rb_2InBr_5 \cdot H_2O$.

Cl was favored in the crystal structure during the change and there were a certain Wyckoff site 8d, which was symmetrically different from other sites 4c laying on the mirror planes in unit cell, tended to acquire more Cl than Br. Water molecule did not have a strong effect on the preferred site or sites for halide substitution. Br might to bond with Sb in the structure. The photoluminescence information provided an idea that $Rb_2InClBr_4 \cdot H_2O{:}Sb$ with a high emission intensity at around 700 nm and major excitation peak around 360 nm might be a potential high efficiency material.

The future work of this project could largely be separated into two parts. One part was to study how the other hydrated phase materials structure changed during mixing or alloying at a site and whether they followed similar pattern or were affected by certain character in symmetry. And the coordinates of Sb and other dopants might need to be confirmed. The other part was that, based on the refined halides ratio of $Rb_2InClBr_4 \cdot H_2O{:}Sb$, relatively higher efficient hydrated phase material could be measured by photoluminescence quantum yield measurements and photoluminescence energy measurements and found by fixing the halides ratios and doping percentage for a more potential material for highly efficient photoluminescence.

7. Reference:

1. Liu, X.; Xu, X.; Li, B.; Liang, Y.; Li, Q.; Jiang, H.; Xu, D. Antimony-Doping Induced Highly Efficient Warm-White Emission in Indium-Based Zero-Dimensional Perovskites. *CCS Chemistry* **2020**, *2* (2), 216–224.
2. Mohammed, O. F. Outstanding Challenges of Zero-Dimensional Perovskite Materials. *The Journal of Physical Chemistry Letters* **2019**, *10* (19), 5886–5888.

3. Knight, A. J.; Herz, L. M. Preventing Phase Segregation in Mixed-Halide Perovskites: A Perspective. *Energy & Environmental Science* **2020**, *13* (7), 2024–2046.
4. Li, X.; Gao, X.; Zhang, X.; Shen, X.; Lu, M.; Wu, J.; Shi, Z.; Colvin, V. L.; Hu, J.; Bai, X.; Yu, W. W.; Zhang, Y. Lead-Free Halide Perovskites for Light Emission: Recent Advances and Perspectives. *Advanced Science* **2021**, *8* (4), 2003334.
5. (international tables) volume a ... - wiley online library. https://onlinelibrary.wiley.com/iucr/itc/Ac/ (accessed Apr 18, 2022).
6. https://icsd.fiz-karlsruhe.de/search/basic.xhtml (accessed Apr 18, 2022).
7. Huang, J.; Chang, T.; Zeng, R.; Yan, J.; Wei, Q.; Zhou, W.; Cao, S.; Zou, B. Controlled Structural Transformation in Sb-Doped Indium Halides a 3 Incl 6 and a 2 Incl 5 ·h 2 O Yields Reversible Green-to-Yellow Emission Switch. *Advanced Optical Materials* 2021, *9* (13), 2002267.
8. Knight, A. J.; Herz, L. M. Preventing Phase Segregation in Mixed-Halide Perovskites: A Perspective. *Energy & Environmental Science* 2020, *13* (7), 2024–2046.
9. Zarick, H. F.; Soetan, N.; Erwin, W. R.; Bardhan, R. Mixed Halide Hybrid Perovskites: A Paradigm Shift in Photovoltaics. *Journal of Materials Chemistry A* 2018, *6* (14), 5507–5537.
10. Jackson D. Majher, Matthew B. Gray, Tianyu Liu, Noah P. Holzapfel, and Patrick M. Woodward, Rb3InCl6: A Monoclinic Double Perovskite Derivative with Bright Sb3+-Activated Photoluminescence. *Inorganic Chemistry* 2020 *59* (19), 14478-14485. DOI: 10.1021/acs.inorgchem.0c02248